Journal of Geophysical Research: Solid Earth

RESEARCH ARTICLE
10.1029/2018JB016445

Fault-Tolerant *b*-Values and Aftershock Productivity

M. T. Page[1] **and N. J. van der Elst**[1]

[1] U.S. Geological Survey, Pasadena, CA, USA

Key Points:
- The Gutenberg-Richter *b*-value does not change with distance from the major mapped faults in Southern California
- Aftershock productivity is also insensitive to distance from major faults
- These results suggest that the faults in Southern California form a highly connected fault network

Supporting Information:
- Supporting Information S1

Correspondence to:
M. T. Page,
mpage@usgs.gov

Citation:
Page, M. T., & van der Elst, N. J. (2018). Fault-tolerant *b*-values and aftershock productivity. *Journal of Geophysical Research: Solid Earth*, *123*, 10,880–10,888. https://doi.org/10.1029/2018JB016445

Received 23 JUL 2018
Accepted 21 NOV 2018
Accepted article online 27 NOV 2018
Published online 21 DEC 2018

Abstract When it comes to smaller earthquakes, are major faults special? Page et al., (2011, https://doi.org/10.1029/2010JB007933) showed that earthquakes near the faults that compose version 3.0 of the Southern California Earthquake Center Community Fault Model (CFM) have a lower Gutenberg-Richter *b*-value than earthquakes elsewhere in Southern California. Here we revisit their result, using newer earthquake data recorded after version 3.0 of the CFM was completed. We find that the correlation between earthquake size and proximity to major faults is not present in the newer seismicity data. This indicates that to some degree, the CFM is overtuned to past seismicity, with some structures related to transient features in seismicity rather than persistent geologic features. We also search for differences in aftershock productivity and foreshock statistics near faults and find that they are also "fault-tolerant"—that is, insensitive to distance from major faults. Our results suggest that the fault system in Southern California is highly connected, since the chance of an earthquake nucleating on or near a major fault versus on a secondary structure is independent of its final size.

Plain Language Summary Individual geologic faults are not isolated. They work together to accommodate the motion between tectonic plates. In this study, we looked at earthquakes that are very close to well-mapped faults such as the San Andreas, as well as earthquakes that occurred far from these faults. We found that earthquakes could be just as large and just as likely to trigger another large earthquake, regardless of whether they were on a major fault or a minor one. Thus, all faults are important; all faults can potentially host a large earthquake, particularly if they "link up" with faults around them.

1. Introduction

In illuminating the structure of the system of faults in Southern California, seismicity is an imperfect lens. Parts of major fault systems like the San Andreas are notably quiet in terms of small earthquakes (Allen, 1968), while other faults are comparatively active. In some areas, seismicity is streaked along seemingly simple, planar structures, while in other areas, it is more diffuse (Hauksson, 2010), presumably because of a more complicated fault system in those areas.

Do earthquakes in these different areas represent distinct populations with different statistics? Fault lengths are known to follow a power-law distribution of lengths (Hirata, 1989; Scholz et al., 1993), and it has been hypothesized that the earthquake size distribution observed in a region can be explained by characteristic earthquakes occurring on many faults of different lengths (Wesnousky, 1999). In this framework, the largest earthquakes preferentially occur on fast-moving, smooth, presumably better connected fault structures, while the smallest earthquakes occur on smaller, less connected faults and are more spatially diffuse. This is consistent with experiments that report higher *b*-values in areas with higher crack density (Mogi, 1962) and the observation that many earthquakes, including aftershocks, occur off of the mainshock fault plane within a broad damage zone (Das & Scholz, 1981; Liu et al., 2003; Ross et al., 2017; Savage et al., 2017).

In probabilistic seismic hazard analysis models, there has been a trend toward including more fault connectivity, although even the recent third Uniform California Earthquake Rupture Forecast (UCERF3) model (Field et al., 2014), which assumes a considerable amount of connectivity between faults, divides seismicity into "on-fault" and "off-fault" components. This is done partly for modeling reasons—since of course even off-fault earthquakes are occurring on faults—but these minor faults are insufficiently characterized to include explicitly in the UCERF3 model. Still, this artificial distinction affects the modeled earthquake rates, since off-fault seismicity is modeled with a different maximum magnitude than on-fault seismicity. In the highest-weighted logic tree branch of UCERF3, the off-fault seismicity has a maximum magnitude of *M*7.6

(and it is even as low as *M*7.2 for another branch). This means that the part of the fault network represented by off-fault seismicity is assumed to be less connected than most mapped faults in the model, which have higher maximum magnitudes.

An alternate possibility is that the California fault system is characterized by extreme connectivity, with moderate and perhaps even the largest earthquakes potentially nucleating in complex, highly fractured areas (e.g., Jackson, 1996; Segall & Pollard, 1980). To test this hypothesis, we use seismicity as a probe of underlying fault connectivity by looking at earthquake magnitudes and triggering productivity near major faults in Southern California to determine whether larger earthquakes in the catalog are more likely to nucleate closer to the major mapped faults than smaller earthquakes.

2. *b*-Values Near Faults

Earthquake sizes in large volumes follow a distribution that is exponential in magnitude and power-law in moment. The number of earthquakes greater than or equal to a given magnitude *M* approximately follows the Gutenberg-Richter distribution, $N(M) = 10^{a-bM}$, where *a* and *b* are constants (Gutenberg & Richter, 1944). The Gutenberg-Richter *b*-value is generally observed to be near unity (Frohlich & Davis, 1993) for large data sets.

When extrapolated from the rate of small earthquakes, small changes in the *b*-value can lead to significant changes in the predicted rate of large earthquakes. The *b*-value is therefore quite important for seismic hazard, and much research has been devoted to looking for systematics in *b*-value variation. Well-established trends in *b*-value variation include a dependence upon faulting mechanism (Schorlemmer et al., 2005), pore pressure (Bachmann et al., 2012; Sammonds et al., 1992), and depth (Mori & Abercrombie, 1997; Spada et al., 2013), as well as, at times, higher *b*-values in volcanic regions (e.g., Roberts et al., 2015; Wiemer & McNutt, 1997; Wiemer et al., 1998).

Other *b*-value work remains somewhat controversial, given that analyses by different research groups can disagree due to different assumptions about the magnitude of completeness or spatial and temporal windows. Apparent *b*-value changes in earthquake sequences prior to mainshocks—which are particularly evident when multiple sequences are stacked relative to mainshock occurrence time—have been shown to be a consequence of aftershock productivity scaling with mainshock magnitude (Utsu, 1972), as they are fit by models that have temporal changes in seismicity rate but not in the magnitude distribution (Helmstetter & Sornette, 2003). Furthermore, nonphysical catalog inhomogeneities, such as seismic network boundaries, can generate a significant signal in the analysis (Kamer & Hiemer, 2015).

Page et al. (2011) analyzed seismicity in Southern California near major faults, as defined by version 3.0 of the Southern California Earthquake Center Community Fault Model (CFM; ; Plesch et al., 2007). One of their results was that seismicity near major faults has a *b*-value about 20% lower than seismicity further from faults. This observation is systematic with distance from the fault (see Figure 1a), statistically significant with minimum magnitudes ranging from 2.5 to 3.1, and robust to short-term aftershock incompleteness (STAI). However, as noted by Page et al. (2011), the latest earthquakes analyzed in the study are roughly coincident with the date of completion (January 2004) of version 3.0 of the CFM. This leaves the potential for circularity in the analysis, if fault locations in the CFM are somehow dependent on the magnitudes of past seismicity.

The CFM is a collaboratively developed model that defines fault geometries using surface traces, seismic reflection profiles, wellbore data, and importantly, seismicity (Plesch et al., 2007). It is this seismicity component in the CFM construction that could allow for the possibility of the fault geometry locations to depend on past earthquake magnitudes. To test for this potential circularity, we repeat the analysis of Page et al. (2011) with newer relocated seismicity in the updated Hauksson et al. (2012) catalog, which has recently been extended to the end of 2017. To avoid earthquakes occurring before version 3.0 of the CFM was completed, we restrict our analysis here to earthquakes that occur in February 2004 and later. Earthquake epicenters and CFM 3.0 faults are shown in Figure 2. Median absolute horizontal and depth errors for $M \geq 2.5$ events in this catalog are 0.3 and 0.7 km, respectively. Median relative location errors are far lower; they are 11 m in both the horizontal direction and in depth.

For earthquakes occurring after the completion of the CFM 3.0, the systematic anticorrelation between *b*-value and distance from the faults disappears (see Figure 1b). By eye, there does not appear to be the strong association between magnitude and distance that is apparent in the earlier data, and, if anything, magnitudes for this data set appear to be *positively* correlated with distance from the faults, which is the reverse of

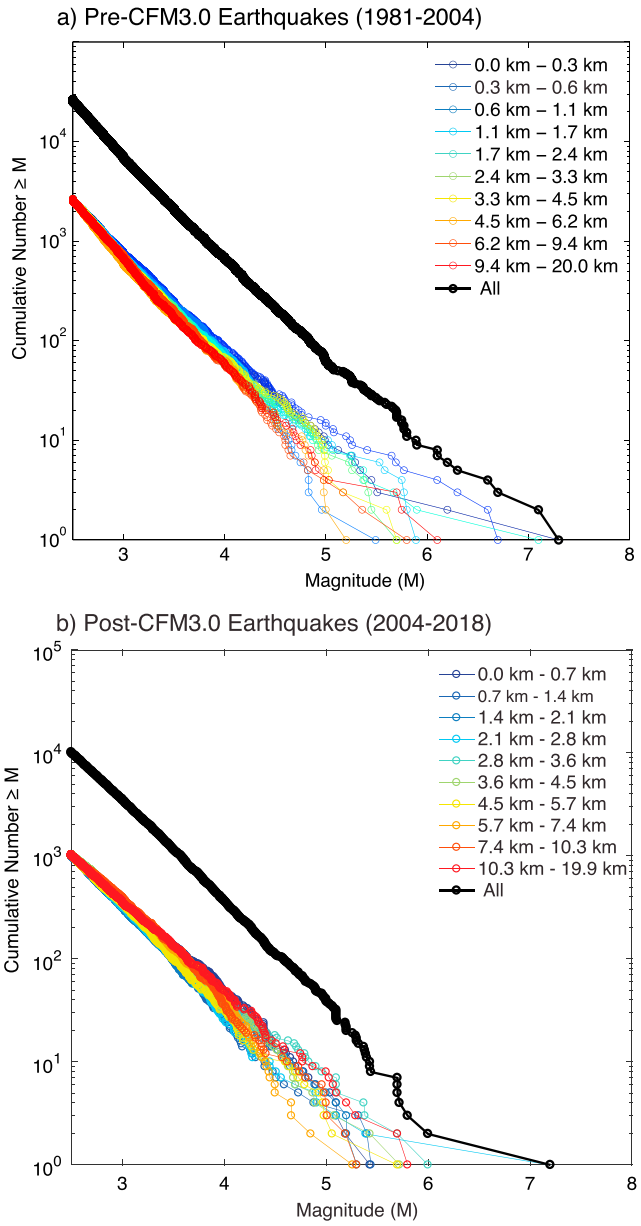

Figure 1. (a) All earthquakes within 20 km of the CFM faults (black) are sorted by distance from the nearest CFM 3.0 fault and then divided into 10 sets of equal size. While the variation in the tails of the subset magnitude distributions is not unusual, there is variation in the magnitude distribution with distance from the faults that can be seen. The nonuniform *b*-values of these subsets as well as the correlation between magnitude and distance to the CFM are both statistically significant. (b) For earthquakes that occurred after this version of the CFM was finalized, there is no longer a negative correlation between magnitude and distance from the nearest modeled fault. CFM = Community Fault Model.

the trend seen in the pre-2004 data. This can also be seen in supporting information Figure S1, which shows maximum-likelihood *b*-value estimates for earthquakes before and after 2004. Even though this result appears to be statistically significant at 95% confidence ($p_{sig} = 0.014$), we interpret this as a spurious correlation, given that it is in the opposite direction as the earlier results (potentially indicating a random sampling component) and earthquake locations are not independent. This latter point is an important effect if there is spatial variation to the *b*-values that is not taken into account by the *p*-value calculation, which is done by leaving earthquake locations constant and randomly reshuffling the earthquake magnitudes. Furthermore, many of the events are part of the 2010 *M*7.2 El Mayor-Cucapah earthquake sequence and outside of California borders and are thus poorly located. If we remove all earthquakes outside California borders, the correlation between

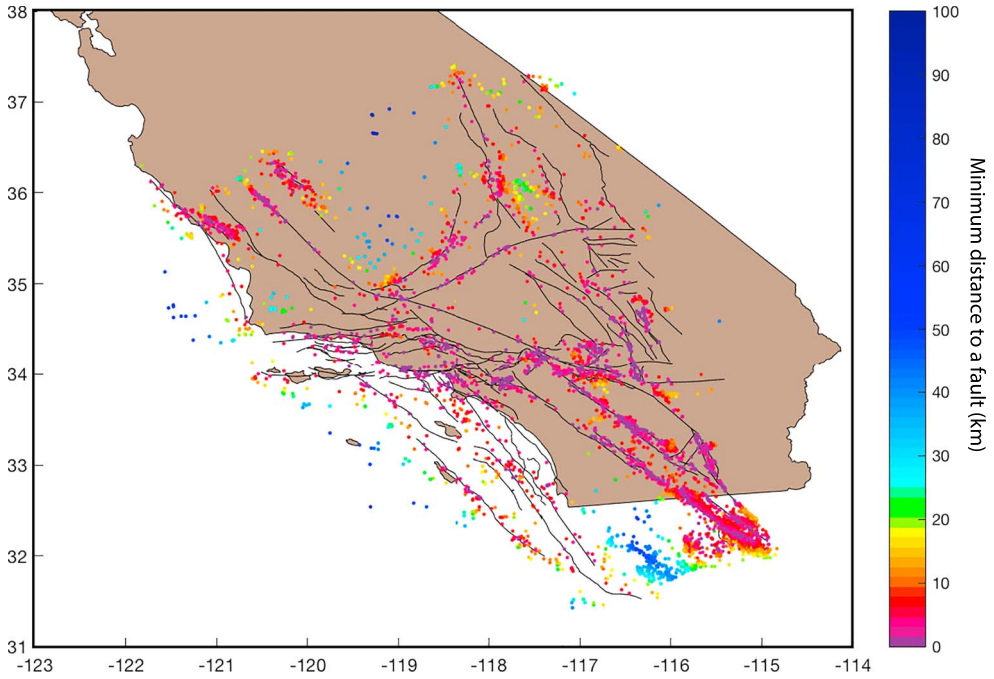

Figure 2. Earthquakes locations from the relocated catalog of Hauksson et al. (2012), from February 2004 to December 2017. Earthquakes are colored by proximity to the nearest fault in the Southern California Earthquake Center Community Fault Model, version 3.0 (Plesch et al., 2007).

magnitude and distance is negative but not statistically significant. Thus, there is not a stable statistically significant relationship between earthquake magnitude and distance from the CFM faults for earthquake data collected after the CFM 3.0 was finalized.

Some of the fault geometries in the CFM are defined using seismicity. This opens the door for circularity in any test that looks for seismicity differences near faults defined after that seismicity occurred. In particular, if CFM structures are drawn to intersect with dense areas of seismicity, they are likely to be preferentially closer to large earthquakes as well, since seismicity is clustered near large earthquakes due to aftershock triggering. This is consistent with the *b*-value signal seen in Page et al. (2011). The fact that this *b*-value variation is not present in seismicity that occurred after the CFM version 3.0 was finalized indicates that at least some fault geometries do not reflect a persistent feature of seismicity. Rather, our results suggest that some CFM structures are picking up features related to short-term aftershock clustering rather than persistent structural features that preferentially host large earthquakes. To create a spurious correlation between fault distance and magnitude, only a small fraction of the CFM structures need be affected. Of the five faults that have the largest pre-2005 negative covariance between fault distance and magnitude, two have geometries defined primarily based on seismicity: "Big Bear rupture," a structure related to the 1992 *M*6.4 Big Bear earthquake, and "Lake Isabella seismicity," a structure running east of Lake Isabella (Plesch, personal communication, Feb. 2017).

There are now more recent versions of the CFM available—as of this writing, the CFM 5.2 is available. In this work we restrict our analysis to the CFM3.0, since using a newer fault model could result in the same circularity problems that affected the analysis of Page et al. (2011).

3. Triggering Productivity Near Faults

The same intuition that leads us to expect a difference in *b*-value near faults leads us to expect a difference in triggering and foreshock statistics near faults. Off the major faults, we are tempted to think of moderate-magnitude earthquakes as occurring on small, poorly connected fault structures, whereas near the major faults, we think of small earthquakes as occurring on secondary "tributary" structures with a higher probability of cascading into a large rupture. In terms of triggering potential, we might therefore expect aftershock sequences near faults to contain more and larger earthquakes than sequences far from major faults.

Table 1
Model Parameters for $M_c = 3.5$

Catalog	μ	a_0	δ	α	p	$log_{10}c$	p_{sig}
Whole	0.08	−2.61	0.02	1.12	1.11	−2.03	0.46
Pre-CFM	0.09	−2.59	−0.09	1.11	1.14	−2.00	0.16
Post-CFM	0.09	−2.58	−0.00	1.12	1.07	−2.17	0.48

Note. CFM = Community Fault Model.

We test for the effect of major faults on triggering statistics in two ways. First, we optimize an epidemic-type aftershock sequence (ETAS) model with a distance-dependent productivity term and evaluate whether it improves the model fit. Second, we use a fault-agnostic ETAS model to identify triggering relationships between events and estimate the rate of foreshocks near to and far from faults.

The ETAS model combines Omori's law with a magnitude-productivity relation to model seismicity as a self-exciting point process (Ogata, 1992):

$$\lambda(t) = \mu + \sum_{t_i<t} 10^{a+\alpha(M_i-M_0)}(t - t_i + c)^{-p}, \tag{1}$$

where the instantaneous earthquake rate $\lambda(t)$ depends on the magnitudes M_i and times t_i of all preceding earthquakes. Parameter μ is the rate of spontaneous earthquakes, parameter a controls the triggering productivity, α controls the scaling of productivity with magnitude, and parameters c and p control the time decay.

To look for a distance dependence to triggering power, we allow a to vary with distance r and optimize for the additional parameter δ:

$$a(r) = a_0 + \delta \log_{10}(r). \tag{2}$$

The results do not change if we try other parameterizations like a step change in productivity or making $a(r)$ linear with distance.

In order to get a reliable estimate of productivity, it is important to take short-term aftershock incompleteness (STAI) into consideration. STAI is a consequence of detection rate saturation in earthquake catalogs due to the presence of continuous, overlapping seismic coda. STAI has been shown to be well-explained by a simple rate-saturation model (Hainzl, 2016a, 2016b), and we modify the ETAS model to correct for STAI through a magnitude-dependent c parameter. Rate saturation causes the c parameter—which describes the length of the early-time plateau in aftershock rate—to appear to scale with mainshock magnitude. The earthquake rate, defined by Omori's law, first falls below the saturation level r_{max} at some time t_c:

$$r_{max} = 10^{a+\alpha(M-M_0)}(t_c + c)^{-p}. \tag{3}$$

Assuming $t_c >> c$, and rearranging for $t_c = c(M)$ gives

$$c(M) = c_0 10^{a/p+\alpha/p(M-M_0)}, \tag{4}$$

where the free parameter c_0 is equal to $r_{max}^{-1/p}$.

We also use a 1-year buffer at the start of each catalog to reduce bias due to the unknown history of seismicity prior to the catalog start (Seif et al., 2016; van der Elst, 2017).

The parameters of the ETAS model are found by maximizing the model likelihood (Ogata, 1992) using the Matlab gradient descent algorithm *fmincon*. We fit the ETAS model with a cutoff at *M*3.0. The ETAS modeling finds very little evidence for variation in productivity with distance, with the distance-dependent productivity term δ estimated to be no more than about 1% of the baseline productivity a_0.

To evaluate the significance of the estimated trend, we randomly reshuffle the distances assigned to the aftershocks and redo the ETAS model estimation 50 times. The reshuffled catalogs give a baseline for the amount of productivity variation that might arise by chance. The significance p_{sig} is then defined as the fraction of

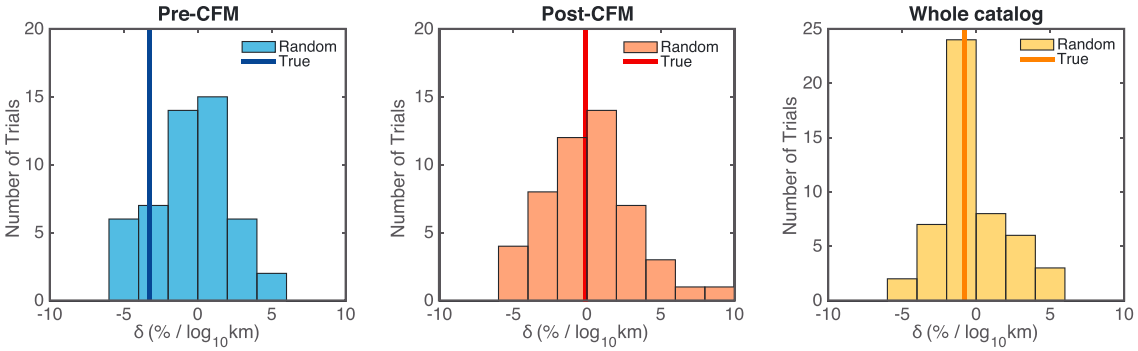

Figure 3. Productivity variation with distance from the nearest CFM fault ($\delta/|a_0|$ from equation (2)). Histograms show the results of 50 trials with randomly reshuffled distances; vertical lines show results using true distances. The true values are indistinguishable from random. CFM = Community Fault Model.

reshuffled catalogs that produce a stronger trend (larger $|\delta|$) than that estimated for the real catalog. For the pre-CFM data, the observed distance dependence is larger than 84% of the simulations, giving $p_{sig} = 0.16$. However, this value is far from statistically significant, and the values for the post-CFM and full data set are close to $p_{sig} = 0.5$, which for a two-tailed test corresponds to maximal insignificance (Figure 3 and Table 1).

Thus, the ETAS results show that for both the pre-CFM and post-CFM catalogs, there is no statistically significant difference in aftershock productivity near and far from major faults. What about the propensity for these aftershocks to be large—in particular, larger than the triggering earthquake itself? Do foreshock statistics vary with distance from a major fault? We now estimate the fraction of events that are foreshocks to a larger event, as a function of distance from the nearest CFM fault.

To evaluate the foreshock rate, we need to assign triggering relationships between earthquakes. We do this using a probabilistic variation of the nearest-neighbor method (Zaliapin et al., 2008). In the nearest-neighbor method, interevent "distance" is defined as

$$R \equiv r^d t^p 10^{-\alpha(M-M_0)}, \tag{5}$$

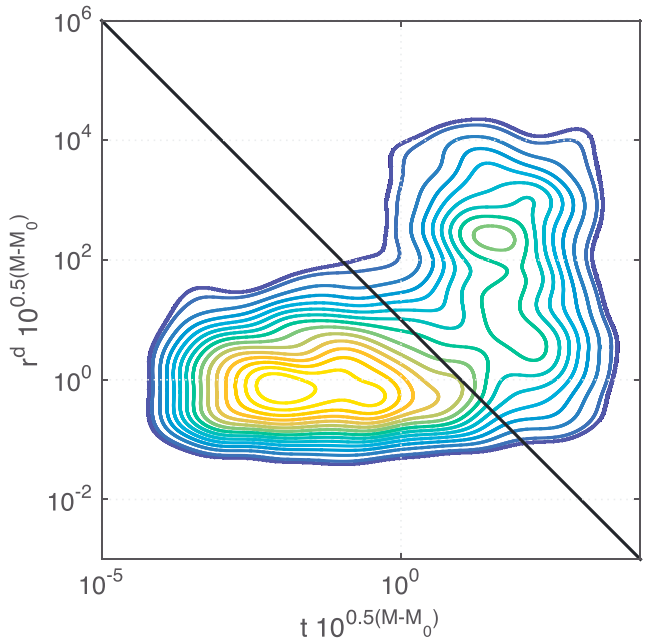

Figure 4. Density of nearest-neighbor distances, following Zaliapin et al. (2008). The horizontal axis is a measure of interevent distance in time and the vertical axis is a measure of interevent distance in space. The diagonal line is the cutoff distance for counting an earthquake as triggered or not; earthquakes in the lower-left quadrant are considered triggered.

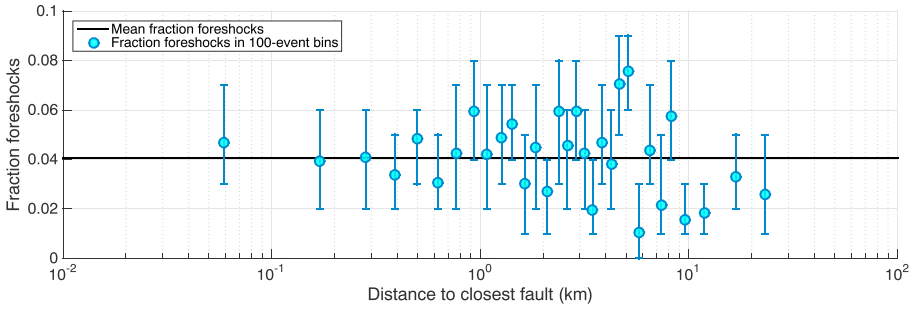

Figure 5. Foreshock rate or fraction of events linked to a subsequent event larger than itself. Each point is for a population of 100 earthquakes, sorted by increasing distance from a Community Fault Model fault. Error bars are 90% confidence ranges from 50 stochastic resamplings of the nearest-neighbor branching structure.

where r and t are the distance and time between any two events, and M is the magnitude of the earlier event. Earthquake "parents" are selected as the events with the smallest nonnegative R. If there are no neighbors for which R falls below some critical value $R\mu$, the event is considered to be spontaneous.

The nearest-neighbor distance has close parallels with the ETAS rate model, and the reader will recognize equation (5) as proportional to the inverse of the per-event ETAS intensity function (equation (1)) with $c = 0$ and the addition of a distance-decay term. We use the analogy with the ETAS model to define a stochastic nearest-neighbor approach, in which we take all of the potential parents with $R < R\mu$ and randomly assign parentage with probability $R_i^{-1} / \sum_i R_i^{-1}$. Randomly resampling the branching structure multiple times (Zhuang et al., 2002) allows us to determine confidence bounds on the foreshock rate in a population, rather than just a point estimate. We use parameters $d = 1.8$ (van der Elst & Shaw, 2015), $p = 1$, and $\alpha = 1$ and impose a cutoff value $R\mu = 10$ (Figure 4).

Figure 5 shows the fraction of events that are linked to aftershocks larger than themselves (the foreshock rate) as a function of distance from the nearest CFM fault. Each point gives the rate and confidence range in

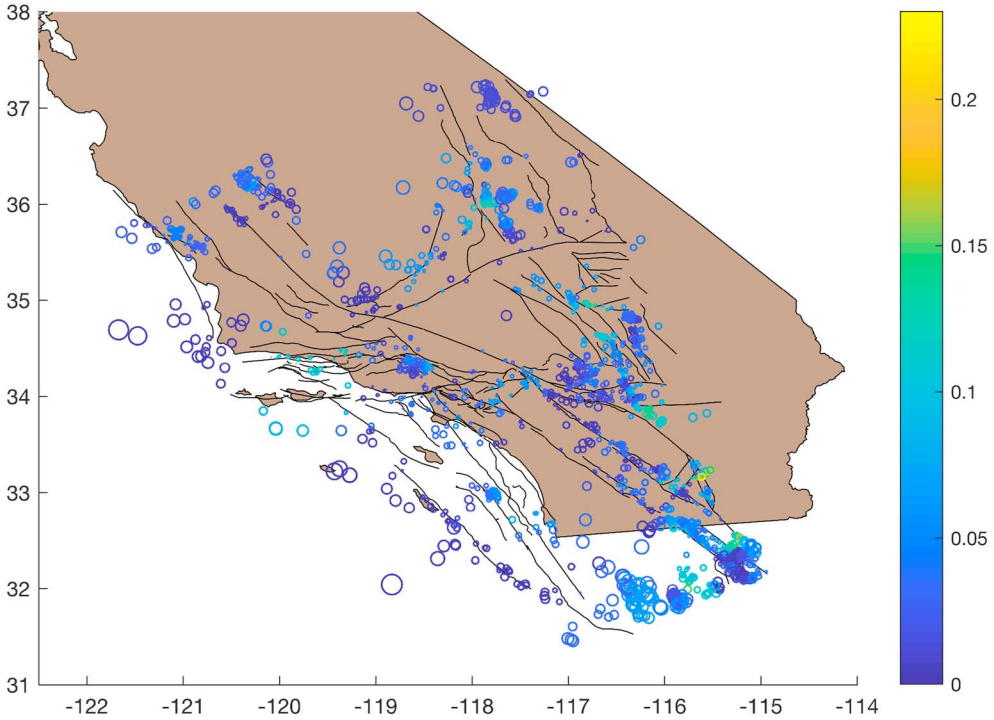

Figure 6. Map of color-coded foreshock rate smoothed over 30-event bins. Community Fault Model faults are in black. Symbol size scales qualitatively with distance from the nearest Community Fault Model fault.

increments of 100 events, sorted by distance. There is no robust trend in foreshock rate with distance from the fault, either before or after the establishment of the CFM.

There is a suggestion of reduced foreshock rates for the most distant population of events (at least 10 km from the closest modeled fault). To investigate whether this might be a meaningful feature of the data, we map the foreshock rate, smoothing over spatial bins of 30 events. The map reveals that lower than average foreshock rates exist in the offshore Continental Borderland (Figure 6). The distance to the closest fault is likely to be overestimated offshore, where geological observations are sparse, making it difficult to attribute this observation to fault proximity as opposed to some other difference between on- and off-shore fault networks.

Finally, these results, which show no variation in foreshock rates as a function of distance from the major faults, corroborate the ETAS-based tests at the beginning of this section, which show no variation in aftershock productivity, since foreshock rates and the number of aftershocks are strongly correlated (Felzer et al., 2004).

4. Discussion and Conclusions

Earthquake magnitude and triggering potential are unaffected by proximity to major faults, which supports the view that the fault system in California is characterized by extreme connectivity; that an earthquake that nucleates within this network of faults is equally likely to grow large regardless of whether it is on a fast-moving, relatively simple structure versus on a small, slow-moving fault strand. Our analysis cannot distinguish whether this is an actual geometric connectivity or an effective one driven by rupture dynamics and the propensity for fault-to-fault jumps (e.g., Harris et al., 2002). Should these results be indicative of a geometric connection, they could potentially constrain estimates of the fractal dimension and fracture density of the fault system (see, e.g., Berkowitz et al., 2000).

Our analysis is restricted to instrumentally recorded earthquakes in Southern California, and, as such, only contains three earthquakes above *M*7. Thus, we cannot rule out a break in scale at high magnitudes where our data set lacks statistical power. However, the connectivity apparent in our data set is also supported by the fact that many recent large earthquakes in continental crust have ruptured multiple faults. Most notably, the 2016 M_w7.8 Kaikōura, New Zealand, earthquake, when imaged by advanced lidar techniques, field mapping, seismological techniques, and InSAR, was found to have ruptured over 20 apparently distinct and disconnected faults (Litchfield et al., 2018). We suggest that ruptures like the Kaikōura earthquake are not the exception, but rather, the rule, and that even the largest earthquakes have a similar complexity to the fault network itself.

Our ability to fully image the fault system is inherently limited by its inaccessibility and fractal nature. While seismicity provides us information about the fault system at depth, that information is incomplete. In the case of the CFM, our results show that parts of the model are likely overtuned to past seismicity. It is important that we do not overinterpret the fault model in terms of its implied connectivity, since we cannot directly image all structures that contribute to the true system-wide connectivity. While current state-of-the-art seismic hazard models such as UCERF3 divide seismicity into on-fault and off-fault earthquakes, this is a false dichotomy—nature cannot tell the difference.

Acknowledgments
We thank Ruth Harris and Jeanne Hardebeck for internal reviews and two anonymous reviewers for journal reviews. The relocated catalog of Hauksson et al. (2012) is available at http://scedc.caltech.edu/research-tools/alt-2011-dd-hauksson-yang-shearer.html. The Community Fault Model (CFM) version 3.0 is available at https://www.scec.org/research/cfm.

References

Allen, C. R. (1968). The tectonic environments of seismically active and inactive areas along the San Andreas Fault System. In W. R. Dickinson & A. Grantz (Eds.), *Proceedings of the Conference on Geologic Problems of the San Andreas Fault System* (Vol. 11, pp. 70–80). Stanford, CA: Stanford University Publications.

Bachmann, C. E., Wiemer, S., Goertz-Allmann, B. P., & Woessner, J. (2012). Influence of pore-pressure on the event-size distribution of induced earthquakes. *Geophysical Research Letters*, *39*, L09302. https://doi.org/10.1029/2012GL051480

Berkowitz, B., Bour, O., Davy, P., & Odling, N. (2000). Scaling of fracture connectivity in geological formations. *Geophysical Research Letters*, *27*(14), 2061–2064. https://doi.org/10.1029/1999GL011241

Das, S., & Scholz, C. H. (1981). Off-fault aftershocks caused by shear stress increase? *Bulletin of the Seismological Society of America*, *71*(5), 1669–1675.

Felzer, K. R., Abercrombie, R. E., & Ekström, G. (2004). A common origin for aftershocks, foreshocks, and multiplets. *Bulletin of the Seismological Society of America*, *94*(1), 88–98. https://doi.org/10.1785/0120030069

Field, E. H., Arrowsmith, R. J., Biasi, G. P., Bird, P., Dawson, T. E., Felzer, K. R., & Zeng, Y. (2014). Uniform California Earthquake Rupture Forecast, Version 3 (UCERF3)—The time-independent model. *Bulletin of the Seismological Society of America*, *104*(3), 1122–1180. https://doi.org/10.1785/0120130164

Frohlich, C., & Davis, S. D. (1993). Teleseismic *b* values—Or, much ado about 1.0. *Journal of Geophysical Research*, *98*(B1), 631–644. https://doi.org/10.1029/92JB01891

Gutenberg, B., & Richter, C. F. (1944). Frequency of earthquakes in California. *Bulletin of the Seismological Society of America*, *4*, 185–188.

Hainzl, S. (2016a). Rate-dependent incompleteness of earthquake catalogs. *Seismological Research Letters*, *87*(2A), 337. https://doi.org/10.1785/0220150211

Hainzl, S. (2016b). Apparent triggering function of aftershocks resulting from rate-dependent incompleteness of earthquake catalogs. *Journal of Geophysical Research: Solid Earth*, *121*, 6499–6509. https://doi.org/10.1002/2016JB013319

Harris, R. A., Dolan, J. F., Hartleb, R., & Day, S. M. (2002). The 1999 İzmit, Turkey, Earthquake: A 3D dynamic stress transfer model of intraearthquake triggering. *Bulletin of the Seismological Society of America*, *92*(1), 245. https://doi.org/10.1785/0120000825

Hauksson, E. (2010). Spatial separation of large earthquakes, aftershocks, and background seismicity: Analysis of interseismic and coseismic seismicity patterns in Southern California. *Pure and Applied Geophysics*, *167*(8–9), 979–997. https://doi.org/10.1007/s00024-010-0083-3

Hauksson, E., Yang, W., & Shearer, P. M. (2012). Waveform relocated earthquake catalog for Southern California (1981 to June 2011). *Bulletin of the Seismological Society of America*, *102*(5), 2239–2244. https://doi.org/10.1785/0120120010

Helmstetter, A., & Sornette, D. (2003). Foreshocks explained by cascades of triggered seismicity. *Journal of Geophysical Research*, *108*, 2457. https://doi.org/10.1029/2003JB002409

Hirata, T. (1989). Fractal dimension of fault systems in Japan: Fractal structure in rock fracture geometry at various scales. *Pure and Applied Geophysics*, *131*(1), 157–170. https://doi.org/10.1007/BF00874485

Jackson, D. D. (1996). The case for huge earthquakes. *Seismological Research Letters*, *67*(1), 3. https://doi.org/10.1785/gssrl.67.1.3

Kamer, Y., & Hiemer, S. (2015). Data-driven spatial b value estimation with applications to California seismicity: To b or not to b. *Journal of Geophysical Research: Solid Earth*, *120*, 5191–5214. https://doi.org/10.1002/2014JB011510

Litchfield, N. J., Villamor, P., Dissen, R. J. V., Nicol, A., Barnes, P. M., Barrell, D. J. A., & Zinke, R. (2018). Surface rupture of multiple crustal faults in the 2016 M_w 7.8 Kaikōura, New Zealand, Earthquake. *Bulletin of the Seismological Society of America*, *108*(3B), 1496–1520. https://doi.org/10.1785/0120170300

Liu, J., Sieh, K., & Hauksson, E. (2003). A structural interpretation of the aftershock "cloud" of the 1992 M_w 7.3 Landers earthquake. *Bulletin of the Seismological Society of America*, *93*(3), 1333. https://doi.org/10.1785/0120020060

Mogi, K. (1962). Magnitude frequency relations for elastic shocks accompanying fractures of various materials and some related problems in earthquakes. *Bulletin of the Earthquake Research Institute, the University of Tokyo*, *40*, 831–853.

Mori, J., & Abercrombie, R. E. (1997). Depth dependence of earthquake frequency-magnitude distributions in California: Implications for rupture initiation. *Journal of Geophysical Research*, *102*(B7), 15081–15090. https://doi.org/10.1029/97JB01356

Ogata, Y. (1992). Detection of precursory relative quiescence before great earthquakes through a statistical model. *Journal of Geophysical Research*, *97*(B13), 19845–19871. https://doi.org/10.1029/92JB00708

Page, M. T., Alderson, D., & Doyle, J. (2011). The magnitude distribution of earthquakes near Southern California faults. *Journal of Geophysical Research*, *116*, B12. https://doi.org/10.1029/2010JB007933

Plesch, A., Shaw, J. H., Benson, C., Bryant, W. A., Carena, S., Cooke, M., & Yeats, R. (2007). Community Fault Model (CFM) for Southern California. *Bulletin of the Seismological Society of America*, *97*(6), 1793–1802. https://doi.org/10.1785/0120050211

Roberts, N. S., Bell, A. F., & Main, I. G. (2015). Are volcanic seismic b-values high, and if so when? *Journal of Volcanology and Geothermal Research*, *308*, 127–141. https://doi.org/10.1016/j.jvolgeores.2015.10.021

Ross, Z. E., Hauksson, E., & Ben-Zion, Y. (2017). Abundant off-fault seismicity and orthogonal structures in the San Jacinto fault zone. *Science Advances*, *3*, 3. https://doi.org/10.1126/sciadv.1601946

Sammonds, P. R., Meredith, P. G., & Main, I. G. (1992). Role of pore fluids in the generation of seismic precursors to shear fracture. *Nature*, *359*, 228–230.

Savage, H. M., Keranen, K. M., Schaff, D. P., & Dieck, C. (2017). Possible precursory signals in damage zone foreshocks. *Geophysical Research Letters*, *44*, 5411–5417. https://doi.org/10.1002/2017GL073226

Scholz, C. H., Dawers, N. H., Yu, J., Anders, M. H., & Cowie, P. A. (1993). Fault growth and fault scaling laws: Preliminary results. *Journal of Geophysical Research*, *98*(B12), 21951–21961. https://doi.org/10.1029/93JB01008

Schorlemmer, D., Wiemer, S., & Wyss, M. (2005). Variations in earthquake-size distribution across different stress regimes. *Nature*, *437*, 539–542. https://doi.org/10.1038/nature04094

Segall, P., & Pollard, D. D. (1980). Mechanics of discontinuous faults. *Journal of Geophysical Research*, *85*(B8), 4337–4350. https://doi.org/10.1029/JB085iB08p04337

Seif, S., Mignan, A., Zechar, J. D., Werner, M. J., & Wiemer, S. (2016). Estimating ETAS: The effects of truncation, missing data, and model assumptions. *Journal of Geophysical Research: Solid Earth*, *122*, 449–469. https://doi.org/10.1002/2016JB012809

Spada, M., Tormann, T., Wiemer, S., & Enescu, B. (2013). Generic dependence of the frequency-size distribution of earthquakes on depth and its relation to the strength profile of the crust. *Geophysical Research Letters*, *40*, 709–714. https://doi.org/10.1029/2012GL054198

Utsu, T. (1972). Aftershocks and earthquake statistics (3): Analyses of the distribution of earthquakes in magnitude, time and space with special consideration to clustering characteristics of earthquake occurrence (1). *Journal of the Faculty of Science, Hokkaido University. Series 7, Geophysics*, *3*(5), 379–441.

van der Elst, N. J. (2017). Accounting for orphaned aftershocks in the earthquake background rate. *Geophysical Journal International*, *211*(2), 1108–1118. https://doi.org/10.1093/gji/ggx329

van der Elst, N. J., & Shaw, B. E. (2015). Larger aftershocks happen farther away: Nonseparability of magnitude and spatial distributions of aftershocks. *Geophysical Research Letters*, *42*, 5771–5778. https://doi.org/10.1002/2015GL064734

Wesnousky, S. G. (1999). Crustal deformation processes and the stability of the Gutenberg-Richter relationship. *Bulletin of the Seismological Society of America*, *89*(4), 1131.

Wiemer, S., & McNutt, S. R. (1997). Variations in the frequency-magnitude distribution with depth in two volcanic areas: Mount St. Helens, Washington, and Mt. Spurr, Alaska. *Geophysical Research Letters*, *24*(2), 189–192. https://doi.org/10.1029/96GL03779

Wiemer, S., McNutt, S. R., & Wyss, M. (1998). Temporal and three-dimensional spatial analysis of the frequency-magnitude distribution near Long Valley Caldera, California. *Geophysical Journal International*, *134*, 409–421.

Zaliapin, I., Gabrielov, A., Keilis-Borok, V., & Wong, H. (2008). Clustering analysis of seismicity and aftershock identification. *Physical Review Letters*, *101*, 18501. https://doi.org/10.1103/PhysRevLett.101.018501

Zhuang, J., Ogata, Y., & Vere-Jones, D. (2002). Stochastic declustering of space-time earthquake occurrences. *Journal of the American Statistical Association*, *97*(458), 369–380. https://doi.org/10.1198/016214502760046925